Non-Oxo Vanadium(IV) Complexes of Aminebis(phenolate) [O,N,O] Donor Ligands and Solution Studies of Isostructural V^{IV} and Mn^{IV} Complexes

Tapan K. Paine,[a] Thomas Weyhermüller,[a] Eckhard Bill,[a] Eberhard Bothe,[a] and Phalguni Chaudhuri*[a]

Keywords: Vanadium / Manganese / EPR spectroscopy / Cyclic voltammetry / Isomerism

Mononuclear non-oxo vanadium(IV) complexes, $[V^{IV}L^{Me}_2]$ (**1**) and $[V^{IV}LtBu_2]$ (**2**), with a tridentate bis(phenol) ligand H_2L bearing the O_2N donor atoms and with either dimethyl or di-*tert*-butyl substituents have been synthesized and the X-ray structures of **1** and **2** are reported. Additionally, **3**, an Mn^{IV} complex $[Mn^{IV}L^{Me}_2]$, and **4**, the anion containing the Mn^{III} center $[Mn^{III}L^{Me}_2]^-$, are discussed. The X-ray structure of **4** present as an anion in **4a**, $[(Me_3tacn)_2Mn^{II}_2(\mu\text{-}OOCCH_3)_3][Mn^{III}L^{Me}_2]$, where Me_3tacn = 1,4,7-trimethyl-1,4,7-triazacyclononane, confirms the magnetic susceptibility results of the high-spin d^4 nature of the manganese center in **4**. The compounds were characterized by elemental analysis, IR, UV/Vis, mass spectrometry, EPR spectroscopy, electrochemical and variable-temperature (2–295 K) magnetic susceptibility measurements. The electrochemical results of **1** and **2** suggest the metal-centered oxidation, i.e. the generation of a V^V–phenolate species, prior to the second oxidation attributable to the formation of a V^V–phenoxyl radical species. Isomerization of the meridional form for the bis(ligand)-metal species to the facial form has been observed for **1** and **3** in solution. The EPR spectroscopic data of **1** and **2** clearly show a considerable increase in the in-plane π bonding, as is expected for a phenolate ligand.

Introduction

We have been exploring the feasibility of using tridentate bis(phenol) ligands,[1] which comprise the three donor atoms [O,X,O], where X = S, Se, P, P=O or N for generating novel transition metal complexes.[2] These types of bis(phenol) ligands are expected to yield homoleptic bis(ligand) non-oxo vanadium(IV) complexes, whose relevance to bioinorganic chemistry has been mentioned quite often in the literature.[3]

It is now well established that vanadium occurs in a variety of biological systems,[3] e.g. in amavadin, a compound isolated from the mushroom *Amanita muscaria*. Amavadin has been shown to contain an eight-coordinate V^{5+} ion without oxo ligands; so-called "bare" or non-oxo vanadium species are still scarce.[4] Non-oxo vanadium centers have also been reported for the cofactor in vanadium nitrogenase. Although the chemistry of oxovanadium(IV) and -(V) complexes is well developed,[5] far less information is available for non-oxo (so-called "bare") complexes, particularly the EPR spectroscopic properties. The vanadyl ion ranks among the most stable of diatomic cations and dominates the chemistry of vanadium. Here we describe two mononuclear octahedral vanadium(IV) complexes ML_2, **1** and **2**, with the ligands H_2L^{Me} and H_2L^{tBu} (X = N) which are depicted in Scheme 1. Our expectation of non-oxo vanadium(IV) complexes was confirmed, as is authenticated by structure determinations, the results of which together with the EPR spectroscopic and electrochemical investigations are described herein. The solution properties of complex **1** and the manganese(IV) complex **3** with the same ligand are also discussed in comparison with the Mn^{III} anion complex **4**. Complex **3** and the anion complex **4** have recently been reported by us.[1c] As the structural characterization of **4** was lacking,[1c] we report it to be the same as the anion in **4a**. Scheme 1 shows the complexes to be described with their labels and the ligands.

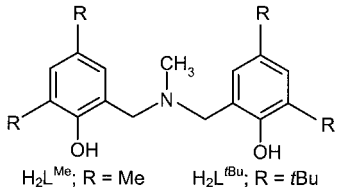

H_2L^{Me}; R = Me H_2L^{tBu}; R = *t*Bu

1 $V^{IV}L^{Me}_2$ **2** $V^{IV}L^{tBu}_2$ **3** $Mn^{IV}L^{Me}_2$ **4** $[Mn^{III}L^{Me}_2]^-$
4a $[(Me_3tacn)_2Mn^{II}_2(\mu\text{-}OOCCH_3)_3][Mn^{III}L^{Me}_2]$
Me_3tacn = 1,4,7-trimethyl-1,4,7-triazacyclononane

Scheme 1

[a] Max-Planck-Institut für Bioanorganische Chemie
Stiftstrasse 34–36, 45470 Mülheim an der Ruhr, Germany
E-mail: chaudh@mpi-muelheim.mpg.de
Supporting information for this article is available on the WWW under http://www.eurjIc.org or from the author.

Results and Discussion

The general method for the synthesis of complexes **1** and **2** involves an anaerobic reaction of $[V^{III}(THF)_3Cl_3]$ with the ligands H_2L and Et_3N as a base in dry acetonitrile. Exposing the resulting solution to air for a while ensures the conversion of V^{iii} to V^{IV} and subsequent storage of the solution under an argon stream, to avoid further oxidation and to concentrate the solution, yields the desired product. The reactions are clean, affording large quantities of pure crystalline products in good yield (50−80%).

$$2\ H_2L^x + V(THF)_3Cl_3 + 4\ Et_3N \xrightarrow[\text{ii) Air}]{\text{i) } CH_3CN,\ Ar} V^{IV}L^x{}_2 + 4\ Et_3NH^+ + 3\ Cl^- + 1\ e^- + 3\ THF$$

X = Me (**1**), *t*Bu (**2**)

Scheme 2

Selected IR data for complexes **1** and **2** are given in the Exp. Sect. There are several strong bands in the region 3000−2800 cm^{-1} due to the ν(C−H) stretchings of the *tert*-butyl or methyl groups. Absence of a strong ν(V=O) stretch at ca. 950 cm^{-1} in **1** and **2** indicates that the complexes are non-oxo species.

EI and ESI mass spectrometry were found to be very important analytical techniques for the characterization of complexes **1** and **2**. The EI mass spectrum of **1** shows a molecular ion peak at *m*/*z* = 645 with only 42% abundance. The base peak at *m*/*z* = 377 is a fragmentation product. The ESI (positive ion mode in CH_2Cl_2) mass spectrum for **2** clearly confirms the composition of the complex showing *m*/*z* (%) = 981 (100).

The electronic spectra (250−1200 nm) of complexes **1** and **2** in CH_2Cl_2 solution primarily consist of two transitions: a band at ca. 550 nm and the second band at ca. 400 nm. The lowest energy band at 550 nm is assigned to phenolate-to-vanadium(IV) CT transitions, by analogy with other reported "bare" vanadium(IV) complexes.[4a−4o] The higher energy transitions at ca. 400 nm, which are absent in the free ligands, are also assigned to the phenolate-to-vanadium(IV) CT transition. There is also a shoulder at ca. 700 nm for complexes **1** and **2**.

Single Crystal X-ray Diffraction Studies

Complexes **1** and **2** are structurally very similar and hence detailed structural aspects of only **1** are discussed here. The molecular structure of **3** has recently been reported.[1c] The structural parameters for the anionic unit **4** are obtained from the structural characterization of $[(Me_3tacn)_2Mn^{II}{}_2(\mu\text{-}OOCCH_3)_3][Mn^{III}L^{Me}{}_2]$ (**4a**), where Me_3tacn represents 1,4,7-trimethyl-1,4,7-triazacyclononane. The cation $[(Me_3tacn)_2Mn^{II}{}_2[\mu\text{-}OOCCH_3)_3]^+$ has been structurally characterized previously.[6]

Molecular Structure of 1

Single crystals of deep blue *mer-trans*-(*N*,*N*)-$[VL^{Me}{}_2]\cdot{}^2/_3CH_3CN$ were obtained from acetonitrile solution by slow evaporation of the solvent. As no substantial differences in bond lengths and angles are found between the crystallographically nonequivalent molecules, only one ORTEP diagram for the structure of compound **1** is displayed in Figure 1, while selected bond lengths and angles are summarized in Table 1.

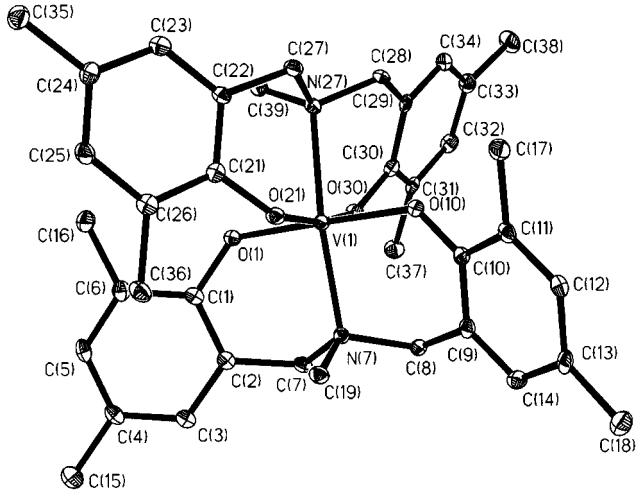

Figure 1. Molecular structure of $[VL^{Me}{}_2]\cdot{}^2/_3CH_3CN$ (**1**)

Table 1. Selected bond lengths [Å] and bond angles [°] for $[VL^{Me}{}_2]\cdot{}^2/_3CH_3CN$ (**1**) (#: center of symmetry-related atoms)

V(1)−O(30)	1.851(2)	O(21)−C(21)	1.353(4)
V(1)−O(21)	1.835(2)	O(30)−C(30)	1.344(4)
V(1)−O(10)	1.919(2)	O(10)−C(10)	1.339(4)
V(1)−O(1)	1.916(3)	O(1)−C(1)	1.346(4)
V(1)−N(27)	2.209(3)	V(1)−N(7)	2.160(3)
O(30)−V(1)−O(21)	168.88(11)	O(30)−V(1)−O(10)	91.46(11)
O(21)−V(1)−O(10)	92.20(11)	O(30)−V(1)−O(1)	87.71(11)
O(21)−V(1)−O(1)	88.84(11)	O(10)−V(1)−O(1)	178.51(11)
O(30)−V(1)−N(27)	83.12(11)	O(21)−V(1)−N(27)	86.59(11)
O(10)−V(1)−N(27)	87.13(11)	O(1)−V(1)−N(27)	94.00(11)
O(30)−V(1)−N(7)	93.31(11)	O(21)−V(1)−N(7)	97.31(11)
O(10)−V(1)−N(7)	88.00(11)	O(1)−V(1)−N(7)	90.81(11)
N(27)−V(1)−N(7)	173.88(11)		
V(2)−O(41)	1.921(3)	O(41)−C(41)	1.342(4)
V(2)−O(41)#	1.921(3)	O(50)−C(50)	1.357(4)
V(2)−O(50)	1.849(2)	V(2)−O(50)#	1.849(2)
V(2)−N(47)#	2.167(3)	V(2)−N(47)	2.167(3)
O(50)−V(2)−O(50)#	180.0	O(41)#−V(2)−O(50)#	90.40(11)
O(41)#−V(2)−O(50)	89.60(11)	O(41)−V(2)−O(50)#	89.60(11)
O(50)−V(2)−O(41)	90.40(11)	O(41#)−V(2)−O(41)	180.0
O(50)#−V(2)−N(47)#	85.35(11)	O(50)−V(2)−N(47)#	94.65(11)
O(41#)−V(2)−N(47)#	91.29(11)	O(41)−V(2)−N(47)#	88.71(11)
O(50)#−V(2)−N(47)	94.65(11)	O(50)−V(2)−N(47)	85.35(11)
O(41)#−V(2)−N(47)	88.71(11)	O(41)−V(2)−N(47)	91.29(11)
N(47)#−V(2)−N(47)	180.00		

The overall geometry around the vanadium ion V(1) is best described as a distorted octahedron with *trans*-positioned nitrogen atoms N(7) and N(27) of the two amine bis(phenolate) ligands. The doubly deprotonated ligand with an [O,N,O] donor set is bound in a meridional manner.

All the phenyl rings attached to the phenolate oxygen atoms are found to be planar, indicating that upon coordination the aromaticity of the phenyl rings is retained. The small distortion from octahedral geometry is mainly caused by the bite angles between the phenolate O atom and the N atom of the $[ONO]^{2-}$ ligand: N(7)−V(1)−O(10) 88.00(11)°, N(7)−V(1)−O(30) 93.31(11)°. The O(30)−V(1)−O(21) and O(10)−V(1)−O(1) angles are 168.88(11) and 178.51(11)°, respectively, while the corresponding N(27)−V(1)−N(7) angle at 173.88(11)° deviates from linearity. All the C−O bond lengths found in compound **1** are normal, the average being 1.345(4) Å. The average V−O and V−N distances of 1.879(3) and 2.185(3) Å fall in the range reported for other structurally characterized mononuclear vanadium(IV) complexes; the V−O bond is a little shorter.[4a] The V−N and V−O bond lengths are in agreement with those of a d^1 V^{IV} complex,[4] which also corroborate with the EPR measurements.

Molecular Structure of 2

This complex is isostructural with complex **1** having overall distorted octahedral geometry around the vanadium ion with two meridionally spanning ligands and two *trans* positioned nitrogen atoms. The ORTEP plot with the atom labeling scheme is shown in Figure 2. The structural parameters are given in Table 2.

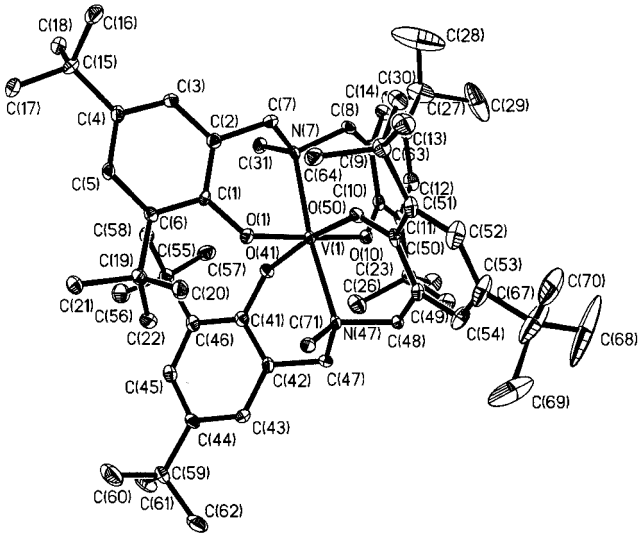

Figure 2. ORTEP representation of $[VLtBu_2]$ (**2**)

Molecular Structure of Complex 4a

The lattice of the crystal used for structural determination consists of discrete $[(Me_3tacn)_2Mn_2(\mu\text{-}OOCCH_3)_3]^+$ and $[ML^{Me}{}_2]^-$ ions. The bond lengths and angles in the cation $[(Me_3tacn)_2Mn_2(\mu\text{-}OOCCH_3)_3]^+$ are comparable (Table 3) with the reported values[6] and hence we have not described the cation in detail. An ORTEP diagram of the anion, **4** in **4a** with the atom labeling scheme is shown in Figure 3. Selected bond parameters are listed in Table 4.

Table 2. Selected bond lengths [Å] and bond angles [°] for $[VLtBu_2]$ (**2**)

V(1)−O(41)	1.854(2)	O(21)−C(21)	1.358(4)
V(1)−O(50)	1.867(2)	O(41)−C(41)	1.359(4)
V(1)−O(1)	1.923(2)	O(10)−C(10)	1.347(4)
V(1)−O(10)	1.938(2)	O(1)−C(1)	1.348(4)
V(1)−N(47)	2.193(3)	V(1)−N(7)	2.159(3)
O(41)−V(1)−O(50)	169.82(10)	O(41)−V(1)−O(10)	87.25(10)
O(41)−V(1)−O(1)	89.31(10)	O(50)−V(1)−O(10)	94.79(10)
O(50)−V(1)−O(1)	89.18(10)	O(10)−V(1)−O(1)	175.20(11)
O(41)−V(1)−N(7)	98.95(11)	O(41)−V(1)−N(47)	87.34(11)
O(50)−V(1)−N(7)	91.11(11)	O(50)−V(1)−N(47)	82.71(10)
O(1)−V(1)−N(7)	89.82(10)	O(1)−V(1)−N(7)	93.56(10)
O(10)−V(1)−N(7)	87.41(10)	O(10)−V(1)−N(47)	89.62(10)
N(7)−V(1)−N(47)	172.91(11)		
V(2)−O(130)	1.862(2)	O(41)−C(41)	1.342(4)
V(2)−O(141)	1.877(2)	O(50)−C(50)	1.357(4)
V(2)−O(101)	1.917(2)	V(2)−O(110)	1.917(2)
V(2)−N(107)	2.174(3)	V(2)−N(147)	2.198(3)
O(130)−V(2)−O(141)	170.58(11)	O(130)−V(2)−O(110)	88.04(10)
O(130)−V(2)−O(101)	88.97(11)	O(141)−V(2)−O(110)	94.84(10)
O(141)−V(2)−O(101)	88.70(10)	O(101)−V(2)−O(110)	175.19(11)
O(130)−V(2)−N(107)	97.16(11)	O(130)−V(2)−N(147)	87.89(10)
O(141)−V(2)−N(107)	91.97(11)	O(141)−V(2)−N(147)	83.15(10)
O(101)−V(2)−N(107)	90.34(10)	O(101)−V(2)−N(147)	93.58(10)
O(110)−V(2)−N(107)	86.30(10)	O(110)−V(2)−N(147)	90.07(10)
N(107)−V(2)−N(147)	173.66(11)		

Table 3. Selected bond lengths [Å] and angles [°] for the complex cation ($[(Me_3tacn)_2Mn_2(\mu\text{-}OOCCH_3)_3]^+$) of **4a**

Mn(2)−O(60)	2.102(3)		
Mn(2)−O(80)	2.102(3)		
Mn(2)−O(70)	2.107(3)		
Mn(2)−N(42)	2.345(3)		
Mn(2)−N(41)	2.359(3)		
Mn(2)−N(40)	2.362(3)		
Mn(3)−O(61)	2.098(3)		
Mn(3)−O(71)	2.107(3)		
Mn(3)−O(81)	2.117(3)		
Mn(3)−N(50)	2.314(3)		
Mn(3)−N(51)	2.332(3)		
Mn(3)−N(52)	2.368(3)		
O(60)−Mn(2)−O(80)	100.5(2)	O(60)−Mn(2)−O(70)	107.02(13)
O(80)−Mn(2)−O(70)	101.23(14)	O(60)−Mn(2)−N(42)	87.48(13)
O(80)−Mn(2)−N(42)	162.59(12)	O(70)−Mn(2)−N(42)	91.01(12)
O(60)−Mn(2)−N(41)	159.79(13)	O(80)−Mn(2)−N(41)	92.80(14)
O(70)−Mn(2)−N(41)	84.93(13)	N(42)−Mn(2)−N(41)	75.84(12)
O(60)−Mn(2)−N(40)	88.74(13)	O(80)−Mn(2)−N(40)	89.20(13)
O(70)−Mn(2)−N(40)	158.90(12)	N(42)−Mn(2)−N(40)	75.41(12)
N(41)−Mn(2)−N(40)	76.21(13)		
O(61)−Mn(3)−O(71)	106.70(11)	O(61)−Mn(3)−O(81)	100.55(12)
O(71)−Mn(3)−O(81)	100.55(12)	O(61)−Mn(3)−N(50)	91.85(11)
O(71)−Mn(3)−N(50)	88.80(11)	O(81)−Mn(3)−N(50)	164.22(11)
O(61)−Mn(3)−N(51)	159.55(11)	O(71)−Mn(3)−N(51)	90.38(11)
O(81)−Mn(3)−N(51)	90.11(11)	N(50)−Mn(3)−N(51)	77.02(10)
O(61)−Mn(3)−N(52)	85.14(12)	O(71)−Mn(3)−N(52)	161.29(11)
O(81)−Mn(3)−N(52)	91.95(12)	N(50)−Mn(3)−N(52)	76.15(11)
N(51)−Mn(3)−N(52)	75.62(11)		

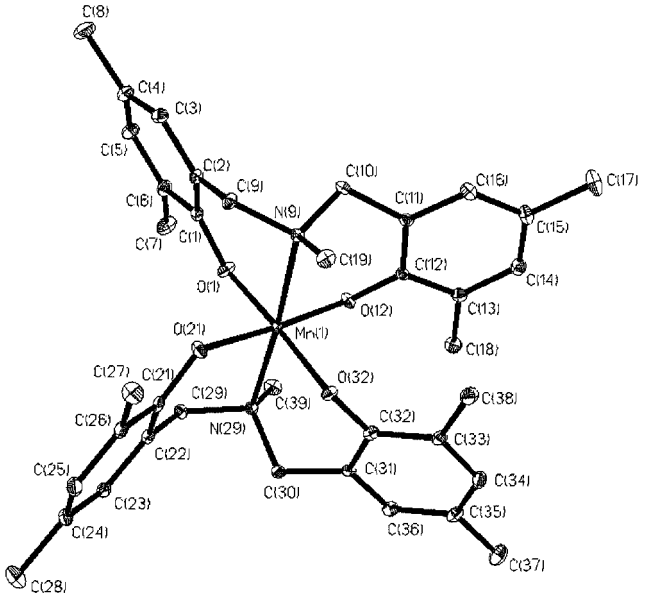

Figure 3. Perspective view of the anionic unit $[MnL_2^{Me}]^-$ (**4**) in **4a**

Table 4. Selected bond lengths [Å] and angles [°] for $[Mn^{III}L_2^N]^-$(**4**) in **4a**

Mn(1)−O(12)	1.913(2)	O(1)−C(1)	1.318(4)
Mn(1)−O(1)	1.919(2)	O(12)−C(12)	1.326(3)
Mn(1)−O(32)	1.920(2)	O(32)−C(32)	1.340(4)
Mn(1)−O(21)	1.926(2)	O(21)−C(21)	1.328(4)
Mn(1)−N(9)	2.317(2)		
Mn(1)−N(29)	2.322(3)		
O(12)−Mn(1)−O(1)	87.52(10)	O(12)−Mn(1)−O(32)	92.35(9)
O(1)−Mn(1)−O(32)	175.80(9)	O(12)−Mn(1)−O(21)	176.50(10)
O(1)−Mn(1)−O(21)	89.96(10)	O(32)−Mn(1)−O(21)	90.33(10)
O(12)−Mn(1)−N(9)	89.34(9)	O(1)−Mn(1)−N(9)	87.64(9)
O(32)−Mn(1)−N(9)	96.56(9)	O(21)−Mn(1)−N(9)	88.13(9)
O(12)−Mn(1)−N(29)	92.24(9)	O(1)−Mn(1)−N(29)	88.14(9)
O(32)−Mn(1)−N(29)	87.66(9)	O(21)−Mn(1)−N(29)	90.10(9)
N(29)−Mn(1)−N(9)	175.43(9)		

Each ligand acts as a facial [O,N,O] donor. In terms of angles within the coordination sphere, MnN_2O_4 is very close to an ideal octahedron. The ranges of *cis* and *trans* angles at the manganese center Mn(1) are 87.5(1)−92.4(1)° and 175.4(1)−176.5(1)°, respectively. The MnO_4 fragment is planar within experimental error, the mean deviation is 0.046 Å.

That the manganese center Mn(1) is in the +3 oxidation state is evident from the axial elongation of the octahedron along the N(29)−Mn(1)−N(9) axis with Mn(1)−N(29) 2.322(3) and Mn(1)−N(9) 2.317(2) Å as is expected for a Jahn−Teller distorted high-spin d^4 ion. The Mn−O [average 1.920(6) Å] and Mn−N [average 2.319(3) Å] distances fall in the range reported for the structurally characterized d^4 Mn^{III} complexes.[7] As expected, the average distances Mn(1)−O and Mn(1)−N are significantly longer than the corresponding bond lengths in complex **3** containing a +4 charged manganese center.[1c]

The anion **4**, being one of the numerous structurally characterized bis(homoleptic) manganese(III) complexes,[7] does not warrant any other special discussion.

Magnetic Susceptibility Studies

Magnetic susceptibility data for polycrystalline samples of complexes **1**, **2** and **4a** were collected over the temperature range 2−290 K in an applied magnetic field of 1 T. Above 10 K the temperature-independent magnetic moments of solids **1** and **2** are 1.69 (± 0.05) μ_B, and 1.70 (± 0.04) μ_B, respectively. These results are consistent with the formulation of the complexes as vanadium(IV) d^1 species (spin-only μ_{eff} = 1.73 μ_B) with no or very small intermolecular coupling and are in complete agreement with the X-ray and EPR spectroscopy results. Simulations (Figure S1 of Supporting Information; see also the footnote on the first page of this article) of the experimental magnetic moment data yield g_v = 1.89, temperature-independent paramagnetism (TIP) = 145 × 10^{-6} emu for **1** and g_v = 1.92, TIP = 200 × 10^{-6} emu for **2**. We note that the *g* values thus evaluated differ from those obtained from the EPR spectroscopic studies (see later).

The magnetic behavior of **4a**, $[(Me_3tacn)_2Mn_2(\mu\text{-}OOCCH_3)_3]^+[MnL_2^{Me}]^-$, is characteristic of an antiferromagnetically coupled complex (Figure 4). At 290 K the μ_{eff} value of 9.24 μ_B ($X_M{\cdot}T$ = 10.686 $cm^3{\cdot}K{\cdot}mol^{-1}$) decreases monotonically with decreasing temperature until it reaches a value of 4.12 μ_B ($X_M{\cdot}T$ = 2.127 $cm^3{\cdot}K{\cdot}mol^{-1}$) at 2 K; this is a clear indication of exchange coupling between two paramagnetic Mn^{II} centers present in the cation of **4a**, with a residual spin moment of ca. 4 μ_B due to the presence of the mononuclear $[MnL_2^{Me}]^-$ anion. The experimental magnetic data were simulated using a least-squares fitting computer program[8] involving three spins $S_1 = {}^5/_2$, $S_2 = {}^5/_2$ and $S_3 = {}^4/_2$ and applying a model in which the coupling between the S_1 and S_2 spins is only prevailing, and there is no exchange interactions between the S_3 and S_1 or S_2 spins. We use the Heisenberg spin-Hamiltonian in the form $\hat{H} = -2J\,\hat{S}_1{\cdot}\hat{S}_2$ for an isotropic exchange coupling between two spins $S_1 = S_2 = {}^5/_2$. The solid line in Figure 4 represents the best fit with the following parameters: J_{12} = −2.14 cm^{-1}, g_1 = g_2 = $g_{Mn^{II}}$ = 2.00, g_3 = $g_{Mn^{III}}$ = 1.95 and *TIP* = 185 ×

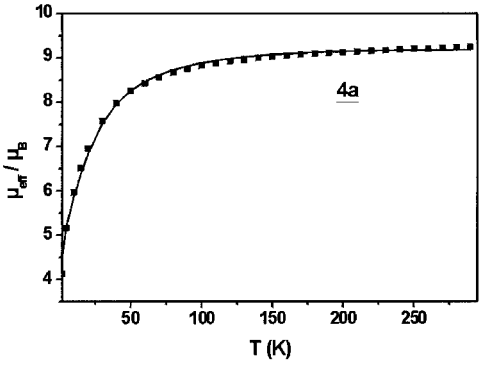

Figure 4. Plots of μ_{eff} vs. *T* for solid **4a**; the solid line represents the best fit of the data to the exchange coupling model

10^{-6} $cm^3 \cdot K \cdot mol^{-1}$. The evaluated antiparallel exchange coupling is very similar to that observed earlier[6] for the cation $[(Me_3tacn)_2Mn_2(\mu\text{-}OOCCH_3)_3]^+$. Thus, the magnetic susceptibility study also corroborates with the structural data of **4a**, whose anion contains the bis(ligand) manganese(III) unit (**4**) with a d^4 high-spin ion.

Electrochemical Results

Cyclic voltammograms (CVs) of complexes **1** and **2** have been measured in CH_2Cl_2 solutions containing 0.1 M nBu$_4$NPF$_6$ as supporting electrolyte at a glassy carbon working electrode and an Ag/AgNO$_3$ reference electrode. Ferrocene (Fc) was used as an internal standard, and the potentials are referenced vs. the ferrocenium/ferrocene couple (Fc^+/Fc). From the voltammograms redox potentials $E_{1/2}$ of the complexes were obtained and are compiled in Table 5.

Table 5. Redox potentials $E_{1/2}$ [V] (vs. Fc^+/Fc) of complexes **1** and **2**, obtained from cyclic voltammograms in CH_2Cl_2 solutions

Complex	$E_{1/2}^{red}$	$E_{1/2}^{ox1}$	$E_{1/2}^{ox2}$
1	−0.882	+0.177	+0.950
2	ca. −0.85[a]	+0.226	+0.875

[a] Slow heterogeneous electron transfer; electrochemically quasi-reversible.

The cyclic voltammogram of **1** displays two reversible and one irreversible wave, whereas that of **2** displays three reversible waves (Figure 5). Coulometric experiments show that the waves are due to one-electron transfer processes. The redox potentials $E_{1/2}$ for the reductions are observed in a narrow range (−0.85 to −0.88 V), irrespective of the nature of the heterodonor, i.e. N, S, Se or P [2] and since, moreover, phenolato ligands are not reduced in this potential range we assign all of these reductions to metal-centered reductions, the V^{III} form of the complexes.

For complexes **1** and **2** we performed controlled potential coulometric experiments at appropriate potentials (at −25 °C) in order to generate the reduced and oxidized forms of the complexes and recorded their electronic spectra. In each of the experiments referring to $E_{1/2}^{red}$ and $E_{1/2}^{ox1}$ the current dropped to background levels when one electron per molecule had passed. The stability of the oxidized and reduced forms was confirmed by recording a CV after the electrolysis or by the recovery of the starting material's electronic spectrum upon voltage reversal. The stabilities of the species were sufficient for the coulometric experiments (duration ca. 30 min at −25 °C).

In all reductions it was found that the broad absorption band which extends from 400 to 700 nm greatly diminishes during electrolysis. Likewise, the changes in the UV/Vis spectra during oxidations exhibit similar features for complexes **1** and **2**: new and very intense absorption grows in two regions, viz. at ca. 300−370 nm (for **1**) or 407 nm (for **2**) and in a second very broad range which extends typically from 500 to 1100 nm. These similarities of the spectral

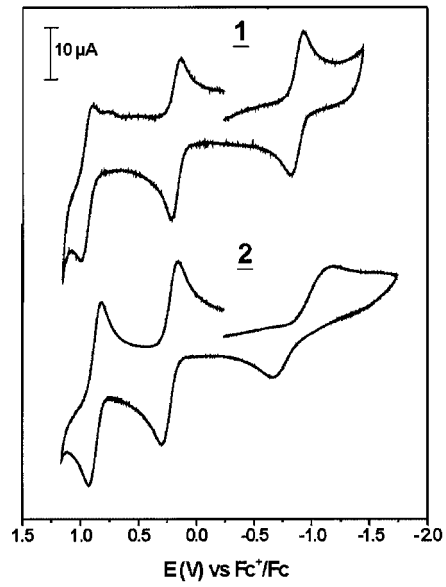

Figure 5. Cyclic voltammograms of complexes **1** and **2** in CH_2Cl_2 solution containing ca. 1 mM complex and 0.1 M nBu$_4$NPF$_6$ (scan rate = 0.2 V/s)

changes provide evidence that the oxidation mechanism is the same for compounds **1** and **2**. Since all monocations (oxidized species) were found to be EPR-silent in the temperature range 2−30 K two mechanisms appear to be feasible: a metal-centered oxidation to a V^V species or formation of an antiferromagnetically coupled V^{IV}−phenoxyl radical system.

However, phenoxyl radicals exhibit a very characteristic electronic spectrum: a band at 400−420 nm and often a single broad band at longer wavelengths with lower intensity. In the present monocations these features are not present: most of the low wavelength bands are at 300−370 nm, they are spread over a much broader range and the bands at higher wavelengths are very intense. Therefore we assign the cations to V^V species.

To gain information about the oxidation mechanism represented by $E_{1/2}^{ox2}$ we performed a $2e^-$ coulometric oxidation on **2**. During the coulometry the current approached a constant value, which indicates that the dication is not stable and there is a concomitant formation and decay of the $2e^-$-oxidized species. However, after two electrons had passed, the frozen solution showed an almost isotropic EPR signal (Figure 6) typical for an organic radical ($S = {}^1/_2$; no vanadium hyperfine coupling; $g_x = g_y = 2.0078$, $g_z = 2.0027$, $\langle g_{iso} \rangle = 2.0061$). Therefore the second oxidation represents the formation of a V^V−phenoxyl radical species.

Solution Properties and EPR Spectroscopy

Although the crystallographically characterized complex was found to be meridional in nature, complex **1** {$[VL_2^{Me}]$}separated out, from the acetonitrile reaction solution, as a mixture of two isomers (*fac* and *mer*). The solid isolated from the reaction solution after 75 h also exists in

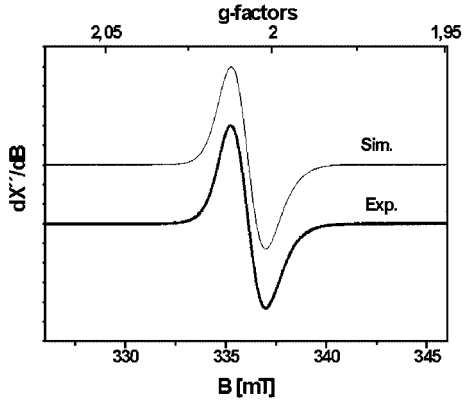

Figure 6. X-band EPR spectrum for the electrochemically $2e^-$-oxidized species of complex **2** at 30 K in CH_2Cl_2; experimental conditions (—): microwave frequency 9.44 GHz, microwave power 0.16 mW, modulation amplitude 6 G; simulations (---): g_{iso} = 2.0061; Gaussian line with angular-dependent line width W = {18, 22, 26} G

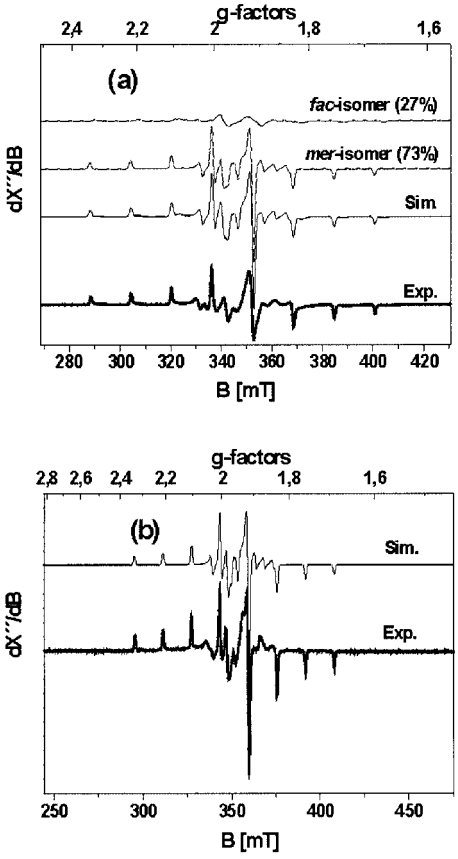

Figure 7. X-band EPR spectra of complex **1** at t = 0, T = 9.9 K (a) and at t = 90 h in CH_2Cl_2 + toluene, T = 33.8 K (b); experimental conditions (—): microwave frequency 9.44 GHz (a), 9.64 GHz (b); microwave power 0.01 μW (a), 0.2 μW (b); modulation amplitude 5 G (a), 5 G (b); simulations for spectrum (a) (---): g = {1.930, 1.960, 1.940}, A = {44, 14, 147} × 10^{-4} cm^{-1} (*fac* isomer); g = {1.932, 1.966, 1.958}, A = {44, 14, 147} × 10^{-4} cm^{-1} (*mer* isomer); Gaussian line with frequency-dependent line width W_f = 80 G (*fac*) and 30 G (*mer*)

two isomeric forms in CH_2Cl_2 solution. When the complex obtained after 75 h was dissolved in CH_2Cl_2 at room temperature followed immediately by LC analysis, both *fac* and *mer* isomers were seen. The LC analyses were performed as a function of time to monitor the change of the relative isomer percentage of **1** in solution.

With time the percentage of the *fac* isomer decreases whereas that of the *mer* isomer increases. 100% *mer* isomer is obtained after 90 h. The LC-MS, clearly indicating the two isomers present in the solution at initial or intermediate times, confirms the presence of only the *mer* form after ca. 90 h. For a qualitative comparison, the UV/Vis spectra of *mer* and *fac* isomers obtained from the LC analyses are provided as Supporting Information (Figure S2).

This change can also be observed in the solution EPR spectra recorded at low temperature. At the very beginning, the spectrum shows a mixture of two isomers, whereas at t = 90 h, only one isomer is seen. The spectrum taken at the beginning can be simulated by considering two isomers in the ratio obtained from the LC analysis (*fac*/*mer* = 27:73). On the other hand, the EPR spectrum of the same solution after 90 h shows only one isomer (meridional) in 100% and can be simulated as seen in Figure 7. The parameters found after simulations with the components x, y and z, respectively, are: g = {1.930, 1.960, 1.940} and A = {44, 14, 147} × 10^{-4} cm^{-1} for the facial isomer and g = {1.932, 1.966, 1.958} and A = {44, 14, 147} × 10^{-4} cm^{-1} for the meridional isomer. The same set of parameters for the meridional isomer was found from the simulation of the EPR spectrum taken after 90 h, containing 100% of the meridional form. Complex **2** on the contrary remains only in the *mer* form presumably due to steric reasons. The EPR spectrum of **2** was simulated with the parameters: g = {1.920, 1.945, 1.954} and A = {50, 10, 146} × 10^{-4} cm^{-1}.

Complexes **1** and **2** belong to the class with a $(d_{xy})^1$ ground state. Six-membered ring formation and steric availability favors the coordination of the ligands in a meridional manner. This results in a small increase in the equatorial σ bonding but considerable increase in the in-plane π bonding.

On the other hand, complex **3**, the Mn^{IV} complex, shows solution behavior in which the nature of the change is the opposite. When complex **3** is dissolved in methanol and the LC analysis is performed, only one isomer is found (100%). This is the *mer* isomer as confirmed from the solid-state crystal structure analysis. But with time the percentage of the *mer* isomer decreases and that of a second isomer (*fac*) increases (Figure 8). After 80 min, there is no more change and the percentage of the two isomers becomes constant with a *fac*/*mer* ratio of 1:4. At this stage the two isomers equilibrate in solution with the K_{eq} value found to be 4.

$$fac \rightleftharpoons mer$$

$$K_{eq} = [mer]/[fac] = 4$$

The isomerization processes for the isostructural **1** and **3** can be rationalized on the basis of the effective ionic radii for V^{IV} and Mn^{IV}. V^{IV}, with a larger ionic radius (0.58 Å)

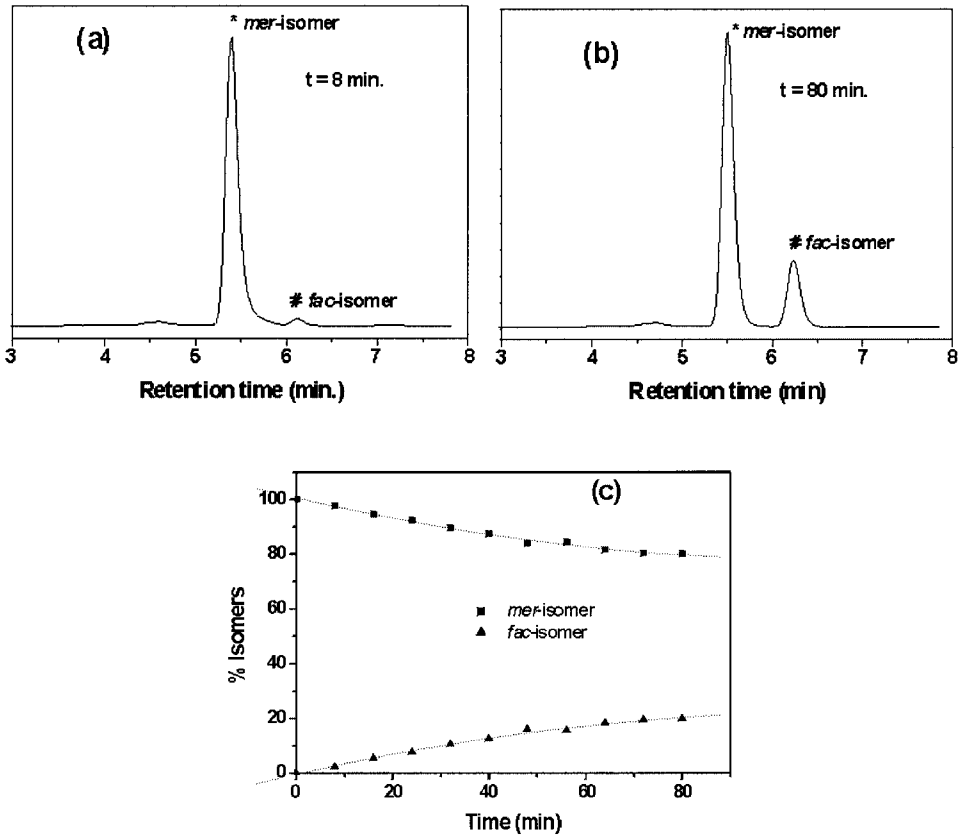

Figure 8. Liquid chromatograms of **3** (a) at t = 8 min and (b) at t = 80 min and (c) change of the isomer percentage with time for complex **3** in CH_2Cl_2 solution; the percentage of isomers is obtained from LC analysis

than that of Mn^{IV} (0.53 Å),[9] is prone to changing the coordination mode of the ligand from facial to meridional because of the steric availability in the meridional form.

This line of argument is in agreement with the observation that the Mn^{III} anion complex **4**, whose structure determination in the solid state shows the presence of only the facial form, also remains facial in solution. Mn^{III} has the largest ionic radius of 0.65 Å amongst these three ions and thus stabilizes the more sterically demanding facial form.

Conclusions

To conclude, the following points of this study deserve particular attention:

(i) The tridentate aminebis(phenolate) ligands with different substituents are capable of generating non-oxo vanadium(IV) complexes, VL_2, in which the ligands are coordinated to the V^{IV} metal center mainly meridionally. A similar geometrical isomer, i.e. meridional, is obtained with the manganese(IV) ions. On the contrary, manganese(III) exclusively yields the facial form. A rationale based on the metal ionic radii has been forwarded to explain the difference in geometrical isomers.

(ii) The investigation emphasizes the observation of the presence of two geometrical isomers, meridional and facial, in solution, albeit the structure determined in the solid state to be meridional.

(iii) Electrochemical measurements indicate that the reversibility of the redox processes is profoundly affected by the substituent on the ligand. Thus, the ligand with *tert*-butyl groups yields reversible redox behavior for the metal complexes. No stabilization of the V^{IV}–phenoxyl radical species has been observed. On the other hand, the formation of a V^{V}–phenoxyl radical complex has been clearly shown by an EPR spectroscopic experiment.

Experimental Section

Materials and Physical Measurements: Commercial grade chemicals were used for the synthetic purposes and solvents were distilled and dried before use. Fourier transform IR spectroscopy on KBr pellets was performed with a Perkin–Elmer 2000 FT-IR instrument. Solution UV/Vis spectra were measured with a Perkin–Elmer Lambda 19 spectrophotometer. Mass spectra were recorded either in the EI or ESI (in CH_2Cl_2) mode with a Finnigan MAT 95 or 8200 spectrometer. Magnetic susceptibilities of the polycrystalline samples were recorded with a SQUID magnetometer (MPMS, Quantum Design) in the temperature range 2–290 K with an applied field of 1 T. The resulting volume magnetization from the sample had its diamagnetic contribution compensated and was recalculated as volume susceptibility. Diamagnetic contributions were estimated for each compound by using Pascal's constants.

Cyclic voltammetry and coulometric experiments were performed using an EG&G potentiostat/galvanostat. X-band EPR spectra were recorded with a Bruker ESP 300E spectrometer equipped with a helium flow cryostat (Oxford Instruments ESR 910), an NMR field probe (Bruker 035M), and a microwave frequency counter HP5352B. Spin-Hamiltonian simulations of the EPR spectra were performed with a program that was developed from the routines of Gaffney and Silverstone[10] and that specifically makes use of the resonance-search procedure based on a Newton−Raphson algorithm as described therein. LC experiments were performed with HPLC instrumentation using a Gilson M305 pump, and the Diode Array Detector (DAD) SPDM 10 AV(Shimadzu Corporation). CH_3OH (0.8 mL/min) was used as eluent through a Nucleodor-5μ-(100A)-C18 column. LC-MS was performed using the above column with a mass spectrometer having a mass-selective detector.

X-ray Crystallographic Data Collection and Refinement of the Structures: Single crystals of **1**, **2** and **4a** were coated with perfluoropolyether, picked up with glass fibers, and mounted on a Nonius Kappa-CCD diffractometer equipped with a cryogenic nitrogen cold stream operating at 100(2) K. Graphite-monochromated Mo-K_α radiation (λ = 0.71073 Å) was used. Intensity data were corrected for Lorentz and polarization effects. The intensity data set of **1** was corrected for absorption with the use of the program Gaussian face-indexed and that for **2** and **4a** were not corrected. The Siemens SHELXTL software package (G. M. Sheldrick, Universität Göttingen[13] was used for solution, refinement, and artwork of the structure, and neutral atom scattering factors of the program were used. All structures were solved and refined by direct methods and difference Fourier techniques. Non-hydrogen atoms were refined anisotropically, and hydrogen atoms were placed at calculated positions and refined as riding atoms with isotropic displacement parameters. Details of data collection and structure refinements are summarized in Table 6. CCDC-211067 (**1**), -211068 (**2**) and -211069 (**4a**) contain the supplementary crystallographic data for this paper. These data can be obtained free of charge at www.ccdc.cam.ac.uk/conts/retrieving.html [or from the Cambridge Crystallographic Data Centre, 12 Union Road, Cambridge CB2 1EZ, UK; Fax: (internat.) + 44-1223/336-033. E-mail: deposit@ccdc.cam.ac.uk].

Ligand Synthesis: The ligands H_2L^{Me},[1c,11] and H_2LtBu[11] were synthesized according to the published procedure. Syntheses of the complexes **3** and the complex anion **4** have recently been reported by us.[1c]

General Method for the Synthesis of V^{IV} Complexes 1 and 2: $V(THF)_3Cl_3$ (0.5 mmol, 0.186 g) was dissolved in a degassed CH_3CN solution (40 mL) of ligand (1 mmol). Et_3N (0.5 mL) was added to the violet solution and the resulting solution was refluxed under argon for 0.5 h. After cooling to room temperature, the solution was opened to air and stirred for 5 min. The solution was then concentrated by passing argon over the surface of the solution to yield a crystalline solid.

Complex $[VL^{Me}_2]\cdot{}^2/_3CH_3CN$ (1): Yield: 0.23 g (68%). $C_{38}H_{46}N_2O_4V\cdot{}^2/_3CH_3CN$ (673.1): calcd. C 70.19, H 7.19, N 5.55, V 7.57; found C 69.9, H 7.1, N 5.5, V 8.7. IR: $\tilde{\nu}$ = 3422 (br), 2902 (s), 1473 (s), 1249 (s), 1158, 813, 596, 559 cm^{-1}. UV/Vis (CH_2Cl_2): λ_{max} (ε) = 362 (6900), 562 nm (9200 $M^{-1}\cdot cm^{-1}$). EI MS: *m*/*z* (%) = 645 (42) [M^+], 377 (100).

Complex [VL*t*Bu$_2$] (2): Yield: 0.26 g (53%). $C_{62}H_{94}N_2O_4V$ (982.38): calcd. C 75.80, H 9.64, N 2.85, V 5.19; found C 75.6, H 9.5, N 2.8, V 5.3. IR: $\tilde{\nu}$ = 3454 (br), 2953−2868 (s), 1465 (s), 1237 (s), 1166,

Table 6. Crystallographic data for $[VL^{Me}_2]\cdot{}^2/_3CH_3CN$ (**1**), [VL*t*Bu$_2$] (**2**) and $[(Me_3tacn)_2Mn_2(\mu\text{-}OOCCH_3)_3][MnL^{Me}_2]$ (**4a**)

	1	**2**	**4a**
Empirical formula	$C_{38}H_{46}VN_2O_4\cdot{}^2/_3CH_3CN$	$C_{62}H_{94}VN_2O_4$	$C_{62}H_{97}Mn_3N_8O_{10}$
Formula mass	673.08	982.33	1279.30
Temperature	100(2) K	100(2) K	100(2) K
Wavelength (Mo-K_α)	0.71073 Å	0.71073 Å	0.71073 Å
Crystal system	monoclinic	monoclinic	monoclinic
Space group	$P2_1/c$	P2(1)	$P2_1/n$
Unit cell dimensions	a = 22.5319(12) Å	a = 11.8937(3) Å	a = 16.3023(6) Å
	b = 16.1089(9) Å	b = 28.1316(9) Å	b = 21.7165(9) Å
	c = 14.5134(9) Å	c = 18.4680(6) Å	c = 18.1744(6) Å
	β = 97.90(1)°	β = 90.57(1)°	β = 93.90(1)°
Volume, Z	5217.8(5) $Å^3$, 6	6178.9(3) $Å^3$, 4	6419.4(4) $Å^3$, 4
Density (calcd.)	1.285 Mg/m^3	1.056 Mg/m^3	1.324 Mg/m^3
Absorption coeff.	0.329 mm^{-1}	0.203 mm^{-1}	0.643 mm^{-1}
F(000)	2146	2140	2720
Crystal size	0.15 × 0.15 × 0.04 mm	0.16 × 0.12 × 0.08 mm	0.27 × 0.16 × 0.14 mm
θ range for data collect.	4.44−26.00°	3.10−24.79°	2.43−30.00°
Index range	$-29 \le h \le 29$,	$-14 \le h \le 14$,	$-22 \le h \le 25$,
	$-20 \le k \le 20$,	$-33 \le k \le 33$,	$-32 \le k \le 33$,
	$-18 \le l \le 18$	$-21 \le l \le 21$	$-25 \le l \le 28$
Reflections collected	33024	105111	83533
Independent reflect.	10170	21124	18699
	[R(int) = 0.0970]	[R(int) = 0.0903]	[R(int) = 0.1217]
Absorption correction	Gaussian, face-indexed	not corrected	not indexed
Data/restraints/parameter	10137/0/638	21123/31/1254	18644/0/748
Goodness-of-fit on F^2	1.019	1.029	1.024
Final R indices [$I > 2\sigma(I)$]	$R1$ = 0.0691,	$R1$ = 0.0548,	$R1$ = 0.0745,
	$wR2$ = 0.1616	$wR2$ = 0.1106	$wR2$ = 0.1675
R indices (all data)	$R1$ = 0.1014,	R = 0.0720,	$R1$ = 0.1069,
	$wR2$ = 0.1798	$wR2$ = 0.1188	$wR2$ = 0.1851
Largest diff. peak/hole	0.652/−0.641 e·$Å^{-3}$	0.597/−0.318 e·$Å^{-3}$	1.261/−1.086 e·$Å^{-3}$

833, 746, 551 cm^{-1}. UV/Vis (CH_2Cl_2): λ_{max} (ε) = 383 (10900), 603 (11800) 814 nm (4100 $M^{-1}\cdot cm^{-1}$, sh). MS (ESI positive ion, CH_2Cl_2): *m*/*z* (%) = 981 (100) [M^+].

Complex [(Me$_3$tacn)$_2$Mn$_2$(μ-OOCCH$_3$)$_3$][MnL$^{Me}_2$] (4a): The ligand (0.15 g, 0.5 mmol) was dissolved in dry methanol (20 mL) and treated with a manganese(III) complex[12] [(Me$_3$tacn)$_2$Mn$_2$(μ-OOCCH$_3$)$_2$(μ-O)](ClO$_4$)$_2$ (0.17 g, 0.25 mmol) and triethylamine (0.5 mL). The resulting red solution was then refluxed under argon for 0.5 h. After cooling to room temperature, the solution was filtered under argon and the isolated solid was dried. X-ray quality crystals were grown from a methanolic solution under a slow sweep of argon. Yield: 0.030 g (10%). $C_{62}H_{97}Mn_3N_8O_{10}$ (1279.30): calcd. C 58.21, H 7.64, Mn 12.88, N 8.76; found C 58.6, H 7.4, Mn 12.5, N 8.5. IR: $\tilde{\nu}$ = 3448 (br), 2990−2814 (s), 1634−1607 (s), 1472 (s), 1314 (s), 1273 (s), 1016, 812, 546·cm^{-1}. UV/Vis (CH_2Cl_2): λ_{max} (ε) = 352 (sh), 427 (2900), 656 (380), 962 nm (200 $M^{-1}\cdot cm^{-1}$). MS (ESI, CH_2Cl_2): *m*/*z* = 629 (positive ion) and 649 (negative ion).

Acknowledgments

Skilful technical assistance of Mrs. H. Schucht, Mr. A. Göbels, Mrs. R. Wagner and Mrs. M. Trinoga is thankfully acknowledged. We are grateful to the German Research Council (DFG) for the financial support (Project: Priority Program Ch 111/2-2).

[1] [1a] P. Chaudhuri, M. Hess, U. Flörke, K. Wieghardt, *Angew. Chem. Int. Ed.* **1998**, *110*, 2217. [1b] R. Siefert, T. Weyhermüller, P. Chaudhuri, *J. Chem. Soc., Dalton Trans.* **2000**, 4656. [1c] T. Weyhermüller, T. K. Paine, E. Bothe, E. Bill, P. Chaudhuri, *Inorg. Chim. Acta* **2002**, *337*, 344. [1d] T. K. Paine, T. Weyhermüller, K. Wieghardt, P. Chaudhuri, *Inorg. Chem.* **2002**, *41*, 6538. [1e] T. K. Paine, E. Rentschler, T. Weyhermüller, P. Chaudhuri, *Eur. J. Inorg. Chem.* **2003**, 3167.

[2] T. K. Paine, PhD thesis, Universität Paderborn, **2002**.

[3] [3a] K. Kustin, G. C. McLeod, *Struct. Bonding (Berlin)* **1983**, *53*, 140. [3b] D. Rehder, *Angew. Chem. Int. Ed. Engl.* **1991**, *30*, 148. [3c] D. Rehder, *Coord. Chem. Rev.* **1999**, *182*, 297. [3d] *Metal Ions in Biological Systems*, vol. 31 ("Vanadium and its Role in Live") (Eds.: H. Sigel, A. Sigel), Marcel Dekker, New York, **1995**. [3e] *J. Inorg. Biochem.* **2000**, *80* (special issue dedicated to biological aspects of vanadium).

[4] [4a] S. R. Cooper, Y. B. Koh, K. N. Raymond, *J. Am. Chem. Soc.* **1982**, *104*, 5092. [4b] U. Auerbach, B. P. C. Della Vedova, K. Wieghardt, B. Nuber, J. Weiss, *J. Chem. Soc., Chem. Commun.* **1990**, 1004. [4c] T. A. Kabanas, A. J. P. White, D. J. Williams, J. D. Woollins, *J. Chem. Soc., Chem. Commun.* **1992**, 17. [4d] A. Neves, A. S. Ceccato, I. Vencato, Y. P. Mascarenhas, C. Erasmus-Buhr, *J. Chem. Soc., Chem. Commun.* **1992**, 652. [4e] T. A. Kabanos, A. M. Z. Slawin, D. J. Williams, J. D. Woollins, *J. Chem. Soc., Dalton Trans.* **1992**, 1423. [4f] S. Bruni, A. Caneschi, F. Cariatia, C. Delfs, A. Dei, D. Gatteschi, *J. Am. Chem. Soc.* **1994**, *116*, 1388. [4g] V. Gergopoulos, S. Jantzen, D. Rodewald, D. Rehder, *J. Chem. Soc., Chem. Commun.* **1995**, 377. [4h] P. R. Klich, A. D. Daniher, P. R. Challen, D. B. McConville, W. J. Youngs, *Inorg. Chem.* **1996**, *35*, 347. [4i] M. Farahbakhsh, H. Schmidt, D. Rehder, *Chem. Commun.* **1998**, 2009. [4j] B. Kang, L. Wenig, H. Liu, D. Wu, L. Huang, C. Lu, J. Cai, X. Chen, J. Lu, *Inorg. Chem.* **1990**, *29*, 4873. [4k] E. Ludwig, H. Hefele, E. Uhlemann, F. Weller, W. Z. Kläui, *Z. Anorg. Allg. Chem.* **1995**, *621*, 23. [4l] H. Hefele, E. Ludwig, E. Uhlemann, F. Weller, *Z. Anorg. Allg. Chem.* **1995**, *621*, 1973. [4m] A. A. Diamantis, M. R. Snow, J. A. Vanzo, *J. Chem. Soc., Chem. Commun.* **1976**, 264. [4n] P. Comba, L. M. Engelhardt, J. M. Harrowfield, G. A. Lawrence, L. L. Martin, A. M. Sargeson, A. H. White, *J. Chem. Soc., Chem. Commun.* **1985**, 174. [4o] A. A. Diamantis, M. Manikas, M. A. Salam, M. R. Snow, E. R. T. Tiekink, *Aust. J. Chem.* **1988**, *41*, 453.

[5] [5a] *Comprehensive Coordination Chemistry* (Eds.: G. Wilkins, R. D. Gillard, J. A. McCleverty), Pergamon Press, England, **1987**, vol. 3, p. 453. [5b] *Encyclopedia of Inorganic Chemistry* (Ed.: R. B. King), John Wiley & Sons, New York, **1994**, vol. 8, p. 4296. [5c] F. A. Cotton, G. Wilkinson, *Advanced Inorganic Chemistry*, 5th ed., John Wiley & Sons, New York, **1988**, p. 665.

[6] K. Wieghardt, U. Bossek, B. Nuber, J. Weiss, J. Bonvoisin, M. Corbella, S. E. Vitols, J. J. Girerd, *J. Am. Chem. Soc.* **1998**, *110*, 7398.

[7] [7a] F. A. Cotton, G. Wilkinson, in *Advanced Inorganic Chemistry*, 5th ed., John Wiley & Sons, New York, **1988**. [7b] *Comprehensive Coordination Chemistry* (Ed.: G. Wilkinson), Pergamon, England, **1987**, vol. 4.

[8] F. Birkelbach, C. Krebs, V. Staemmler, Bochum, Germany, **1997**, unpublished results.

[9] R. D. Shannon, *Acta Crystallogr., Sect. A* **1976**, *32*, 751.

[10] B. J. Gaffney, H. J. Silverstone, in *EMR of Paramagnetic Molecules* (Eds.: L. J. Berliner, J. Reuben), Plenum Press, New York, **1993**, vol. 13.

[11] N. N. Timosheva, A. Chandrasekharan, R. O. Day, R. R. Holmes, *Inorg. Chem.* **1998**, *37*, 4945.

[12] K. Wieghardt, U. Bossek, D. Ventur, J. Weiss, *J. Chem. Soc., Chem. Commun.* **1995**, 347.

[13] ShelXTL V.5: Siemens Analytical X-ray Instruments, **1994**; ShelXL 97: G. M. Sheldrick, University of Göttingen, **1997**.

Received June 25, 2003
Early View Article
Published Online November 4, 2003

